Excitation Energy Transfer in Chlorosomes of Green Bacteria: Theoretical and Experimental Studies

Zoya Fetisova,* Arvi Freiberg,# Koit Mauring,# Vladimir Novoderezhkin,* Alexandra Taisova,* and Kiu Timpmann#

*A. N. Belozersky Institute of Physico-Chemical Biology, Moscow State University, 119899 Moscow, Russia, and #Institute of Physics, Estonian Academy of Sciences, 202400 Tartu, Estonia

ABSTRACT A theory of excitation energy transfer within the chlorosomal antennae of green bacteria has been developed for an exciton model of aggregation of bacteriochlorophyll (BChl) *c* (*d* or *e*). This model of six exciton-coupled BChl chains with low packing density, approximating that in vivo, and interchain distances of ~2 nm was generated to yield the key spectral features found in natural antennae, i.e., the exciton level structure revealed by spectral hole burning experiments and polarization of all the levels parallel to the long axis of the chlorosome. With picosecond fluorescence spectroscopy it was demonstrated that the theory explains the antenna-size-dependent kinetics of fluorescence decay in chlorosomal antenna, measured for intact cells of different cultures of the green bacterium *C. aurantiacus*, with different chlorosomal antenna size determined by electron microscopic examination of the ultrathin sections of the cells. The data suggest a possible mechanism of excitation energy transfer within the chlorosome that implies the formation of a cylindrical exciton, delocalized over a tubular aggregate of BChl *c* chains, and Forster-type transfer of such a cylindrical exciton between the nearest tubular BChl *c* aggregates as well as to BChl *a* of the baseplate.

INTRODUCTION

The primary photophysical processes of light energy conversion in in vivo photosynthesis are extremely efficient because of the strict optimization of the photosynthetic apparatus structure according to the functional criterion (Fetisova, 1994). One of the structural optimizing factors is oligomerization of pigments both of the antenna and of the reaction center (Fetisova et al., 1989).

Oligomerization of pigments has its origin in intrinsic donor–acceptor properties of chlorophylls, which make possible self-aggregation of these pigments in vitro and in vivo (Smith et al., 1983). These key properties of chlorophylls allow for the realization of a basic principle of life, i.e., the self-organization of the order that is vital for all living systems because only ordered systems can be optimized. It is very likely that chlorophylls were chosen by Nature as molecules engaged in the primary processes of light energy storage primarily because they possess these properties.

The most amazing example of long-range ordered natural light-harvesting structures is the chlorosome of green bacteria, the largest among all the known antenna systems (more than 1000 molecules of bacteriochlorophyll (BChl) per reaction center in sulfur green bacteria (Olson, 1980)).

The chlorosome contains several thousand main light-harvesting pigments (BChl *c*, *d*, or *e*, depending on species) associated with six subunits organized hexagonally in the form of hollow cylinders (called rod elements) each 5–10 nm in diameter and approximately 100–250 nm long. The chlorosome contains 10–30 such rods running the length of each chlorosome. Each rod element exhibits the substructure with 6-nm periodicity along its long axis (Olson et al., 1977; Staehelin et al., 1978; 1980; Golecki and Olze, 1987).

In the past decade, the chlorosome antenna structure and function in different green bacteria have been extensively studied (for reviews see Van Grondelle et al., 1994; Savikhin et al., 1994). A major question about the mechanism of excitation energy transfer within the chlorosome, however, is still open. It is the answer to this question that is the main goal of the present work. This problem is most acute in view of the oligomeric organization of chlorosomal pigments, because until now only the theory of excitation energy transfer (EET) between the dimers in photosynthetic antennae had been developed (Struve, 1996). Besides, there is no adequate molecular model of the chlorosome structure compatible with key experimental results obtained on the in-vivo systems. Thus, the first problem is the search for such a model.

The strong orientational ordering of the near-infrared transition dipoles of BChl *c* was demonstrated both in situ (Fetisova et al., 1988) and in isolated chlorosome–membrane complexes (Fetisova et al., 1986). Similar results were obtained for isolated chlorosomes (Van Dorssen et al., 1986; Van Amerongen et al., 1988; Griebenow et al., 1991; Lin et al., 1991; Matsuura et al., 1993; Mimuro et al., 1994). This suggests that an elementary BChl aggregate has the form of at least a quasi-linear chain.

This interesting phenomenon has attracted considerable interest and given rise to studies of the supramolecular

Received for publication 14 December 1995 and in final form 11 April 1996.

Address reprint requests to Dr. Zoya G. Fetisova, A. N. Belozersky Institute of Physio-Chemical Biology, Building "A," Moscow State University, 119899 Moscow, Russia. Tel.: 07-095-939-53-63; Fax: 07-095-939-31-81; E-mail: fzg@pa.genebee.msu.su.

Abbreviations used: BChl, bacteriochlorophyll; CD, circular dichroism; EET, excitation energy transfer; HBS, hole-burning spectrum; ZPH, zero-phonon hole; ZPL, zero-phonon line.

0006-3495/96/08/995/16 $2.00

organization of the chlorosome. Plausible molecular models of chlorosomal BChl aggregates have been the subject of numerous experimental and theoretical investigations (see the special issue on green and heliobacteria, *Photosynth. Res.* 41(1), 1994), and some models are thought to be good models of the in vivo chlorosome structure (Smith et al., 1983; Mimuro et al., 1989, 1994; Lin et al., 1991; Alden et al., 1992; Holzwarth and Schaffner, 1994; Nozawa et al., 1994; Feiler et al., 1994; Krasnovsky and Bystrova, 1980). These models, based on the pigment–pigment interaction concept, were developed by use as the main criteria the red-shift value of optical spectra of oligomeric BChl models compared with monomeric ones, the strong orientational ordering of the Q_y transition dipoles, the five-coordinated nature of BChl aggregates, the chemical shift values that are due to hydrogen bonding, and rodlike arrangement of BChl aggregates chains.

From the point of view of density of BChl chain packing, all the models proposed earlier can be classified into two groups, which essentially characterize two limiting cases:

i) Noninteracting BChl chains (linear chains, linear antiparallel double chains, and zig-zag chains) (for reviews see Alden et al., 1992; Nozawa et al., 1994).
ii) Strongly exciton-coupled BChl chains with a high density of packing owing to self-aggregation of pigments into an entire macrocycle network (tubular arrangement of tightly packed single (Holzwarth and Schaffner, 1994) or double (Nozawa et al., 1994) BChl chains).

The exciton level structure of an aggregated model is extremely sensitive to the density of the BChl packing. Information about the exciton level structure of natural BChl *c* and *e* aggregates is available from recent spectral hole-burning studies performed on three species of intact cells from both families of green bacteria, *Chlorobiaceae* and *Chloroflexaceae* (Fetisova and Mauring, 1992, 1993; Fetisova et al., 1994, 1995). The experiments have shown the following features of hole-burning spectra (HBSs), which are fundamentally similar for all species investigated:

i) The total width of a HBS is always equal to that of a preburned spectrum (350–830 cm^{-1}, depending on species), exceeds the inhomogeneous width (90–100 cm^{-1}), and does not depend on temperature. This means that the large homogeneous width of the absorption spectrum is determined by exciton levels rather than by phonon wings, i.e., exciton–phonon coupling is weak.
ii) At burning wavelengths within the long-wavelength side of excitation band, a HBS consists of a resonant zero-phonon hole (ZPH) corresponding to the lowest exciton level (1600–2000 cm^{-1} red shifted with respect to the monomer absorption maximum) and of a broad nonresonant hole corresponding to the higher levels broadened because of relaxation. The integral intensity of a ZPH is considerably less than that of the broad component. Thus, the higher exciton level, blue shifted by 200–400 cm^{-1} (depending on species) with respect to the lowest one, has the greatest part of the total oscillator strength.

We demonstrate that neither the models of noninteracting BChl chains nor tubular models with tightly packed BChl chains, postulating self-aggregation of the pigments into an entire macrocycle network, exhibit the in vivo exciton level structure of BChl aggregates revealed by spectral hole-burning experiments on intact cells of green bacteria. Alternatively, new models of linear exciton-coupled BChl chains with a low packing density, approximating that in vivo, are generated to yield the main spectral features found in natural antennae.

For these new models, a theory of EET within the chlorosome is developed. The analytical expression for the time constant of chlorosomal BChl fluorescence decay as a function of the chlorosome size is obtained. Finally, using picosecond fluorescence spectroscopy, we demonstrated that this theoretical dependence agrees well with experimental dependences, measured for intact cells of different cultures of the green bacterium *Chloroflexus aurantiacus* with the different chlorosome size determined by electron microscopic examination of the cells.

The data suggest a possible mechanism of EET within the chlorosome, namely, the inductive-resonance-type transfer of a cylindrical exciton delocalized over tubular BChl *c* aggregate structures.

MATERIALS AND METHODS

All experiments were performed on intact cells of the filamentous nonsulfur thermophilic green bacterium *Chloroflexus aurantiacus* strain Ok-70-fl (collection of Leiden University, Leiden, The Netherlands) used in their own growth medium under strictly anaerobic conditions. Cells were cultivated at 55°C under anaerobic conditions in light. We adjusted the different size of chlorosomal antennae (i.e., the different ratios of BChl *c*/BChl *a*) by changing the growth rate (Oelze and Fuller, 1987)) and by inhibiting the formation of BChl *c* with gabaculine (0.7-, 1.6-, and 2.2-μM concentrations were used) according to the method of Oelze (1992).

Electron microscopic observations were made with Hitachi-11 or Hitachi-12 electron microscopes operating at 75 kV. For electron microscopic examination the cells were fixed for 30 min in the culture medium at 55°C by addition of 25% glutaraldehyde to a final concentration of 1% and then at room temperature for 60 min. The samples were postfixed with 1% OsO_4 for 90 min, embedded in Epon-812, and ultrathin sectioned by standard methods (Staehelin et al., 1978). Micrographs of the ultrathin sections were used for morphometric measurements (magnification 50,000 × 10). Histograms of chlorosomes heights were obtained for cells grown under different conditions. We calculated the number of layers of rod elements in a chlorosome by using the results reported by Staehelin et al. (1978).

Absorption spectra of intact cells were recorded at room temperature with a Hitachi-557 spectrophotometer. Circular dichroism spectra of intact cells were measured with a Mark III CD spectrometer (Yvon Jobin, Paris, France).

Spectrally resolved fluorescence measurements for intact cells of *Chloroflexus aurantiacus* were made with a picosecond spectrochronograph described by Fetisova et al. (1988). Briefly, the picosecond pulse source was a mode-locked cw Rhodamine 590 dye laser (pulse duration 3 ps), synchronously pumped at 76 MHz by a Nd:YAG laser (Ontares model, Coherent, USA). Emission, viewed at an angle of 90° to the exciting beam (in the reflection mode), was filtered by two single-grating monochromators (Lomo MDR-2, St. Petersburg, Russia), combined in a subtractive

dispersion mount to avoid extra pulse broadening (bandwidth 4 nm), and registered with a homemade synchroscan streak camera. The time resolution of the measuring system was 10 ps. Data were recorded and processed with a PC IBM computer supported by a B&M Spectronik OSA 500 optical multichannel analyzer with a SIT vidicon.

THEORY OF BACTERIOCHLOROPHYLL AGGREGATE SPECTROSCOPY

In this section we present the exciton theory of absorption spectra and HBSs of chlorosomal antennae for different models of BChl aggregation, including all hitherto proposed molecular models of the chlorosome. We develop our theory of BChl aggregate spectra by using the standard approach to the exciton-phonon problem in molecular crystals (Davydov, 1971) generalized to the case of finite-sized aggregates.

LOW-TEMPERATURE ABSORPTION SPECTRA

Noninteracting single BChl chain models

In this section we consider the BChl *c* aggregates that have the form of a one-dimensional (or quasi-one-dimensional) single chain with chiral architecture (Fig. 1*A*). We assume symmetry with respect to translations, i.e., the energy of interaction between the $(n-1)$th and the nth molecules is equal to that between the nth and the $(n+1)$th molecules. The orientation of the BChl transition dipole moment $\mathbf{d}_n$ is characterized by angles $(n\phi)$ and ψ, where ψ is the angle between $\mathbf{d}_n$ and the long axis of the aggregate **z**; $(n\phi)$ characterizes the orientation of the projection of vector $\mathbf{d}_n$ to the **xOy** plane (ϕ is the azimutal step angle). Angle ξ characterizes the rotational motion of BChl molecules around $\mathbf{d}_n$.

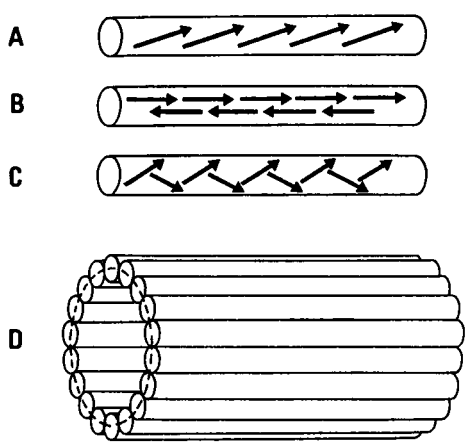

FIGURE 1 BChl aggregation models: (*A*) Single-chain model. The arrows show the transition dipoles of the BChl molecules. The directions of the transition dipoles correspond to molecular wave functions with any fixed phase (the same for all molecules). This means that the relative orientation of the arrows corresponds to the relative orientation of the molecules in an aggregate. (*B*) Antiparallel double-chain model. (*C*) Zigzag chain model. (*D*) Tubular model with a high density of strongly exciton-coupled BChl chain packing. Each elementary cylinder in the *D* model contains a single or double BChl chain.

In our description directions of transition dipoles $\mathbf{d}_n$ correspond to molecular wave functions with any fixed phase (the same for all molecules). This means that the relative orientation of the arrows in Fig. 1 corresponds to the relative orientation of the molecules in an aggregate.

The Hamiltonian for the linear aggregate can be written as (Chesnut and Suna, 1963)

$$H = \sum_{n=1}^{N} (\Delta E + D_n) B_n^+ B_n + \sum_{n=1}^{N-1} M_{n,n+1}(B_n^+ B_{n+1} + B_{n+1}^+ B_n). \tag{1}$$

Here ΔE is the electronic excitation energy of the isolated BChl molecule, D_n is the change of energy of the nth molecule under electronic excitation, $M_{n,n+1}$ is the matrix element of resonant interactions between molecules n and $(n+1)$, and B_n^+ and B_n are the excitation creation and destruction operators, respectively, at the nth site. In general, electronic excitations of BChl in light-harvesting complexes are coupled with phonon modes and intramolecular vibrations. For example, Chl *a* molecules in PSI-200 particles of spinach are coupled with 41 intramolecular vibrational modes (with frequencies distributed from 250 to 1500 cm^{-1}) and the phonon modes (Gillie et al., 1989). The Huang–Rhys factors for the intramolecular modes are small (less than 0.044), whereas the Huang–Rhys factor for the phonon mode (22 cm^{-1}) is much larger (~0.8) (Gillie et al., 1989). We assume a similar relation between coupling parameters for chlorosomal BChl *c*. That is why we consider the coupling with the phonon modes, ignoring the intramolecular vibrations. In our exciton–phonon description only the librational modes are accounted for. Deformation of the lattice then refers to the orientation displacement. (Deformation that is due to the translational displacement can be accounted for in a similar manner.) The orientation of the nth molecule is characterized by angles $(n\phi + \phi_n)$, $\psi + \psi_n$, and $\xi + \xi_n$, where $(n\phi)$, ψ, and ξ correspond to the equilibrium orientations of molecules without electron–phonon coupling. In the case of a linear electron–phonon coupling

$$\begin{aligned} D_n &= D + D^\phi \phi_n + D^\psi \psi_n + D^\xi \xi_n, \\ M_{n,n+1} &= M + M^\phi(\phi_n - \phi_{n+1}) + M^\psi(\psi_n + \psi_{n+1}), \\ M &= d^2/R^3(-2 + \sin^2\psi(2 + \cos\phi)), \\ M^\phi &= d^2/R^3(\sin^2\psi \sin\phi); \\ M^\psi &= d^2/R^3(\sin 2\psi(2 + \cos\phi)/2), \end{aligned} \tag{2}$$

where R is the intermolecular distance and d is the transition-dipole moment of the BChl monomer. Angles ϕ_n, ψ_n, and ξ_n can be replaced by phonon creation and destruction

operators b_{qs}^{+} and b_{qs}:

$$\phi_n = \sum_{qs} e_{qs}^{\phi} a_{qs}^{\phi} (b_{qs}^{+} + b_{qs}) c_n^q, \qquad a_{qs}^{\phi} = (h/2I_{\phi}\Omega_{qs})^{1/2},$$

$$c_n^q = [2/(N+1)]^{1/2} \sin(\vartheta nq),$$

$$q = 1, 2, \ldots N, \qquad \vartheta = \pi/(N+1), \tag{3}$$

where e_{qs}^{ϕ} is the ϕ component of the unit vector of polarization corresponding to optical phonon branch s (s = 1, 2, 3) and wave number q, Ω_{qs} is the phonon librational frequency, and I_{ϕ} is the mass coefficient (moment of inertia) corresponding to coordinate ϕ. The expressions for ψ_n and ξ_n are similar to Eq. 3. The Hamiltonian (Eq. 1) can be rewritten in the form

$$H_{ex} = \sum_{n=1}^{N} (\Delta E + D) B_n^{+} B_n + \sum_{n=1}^{N-1} M(B_n^{+} B_{n+1} + B_{n+1}^{+} B_n),$$

$$H'_{int} = \sum_{n=1}^{N} \sum_{qs} \chi_{qs} B_n^{+} B_n (b_{qs}^{+} + b_{qs}),$$

$$H''_{int} = \sum_{n=1}^{N-1} \sum_{qs} (f_{qs}^{n} + f_{qs}^{n+1})(B_n^{+} B_{n+1} + B_{n+1}^{+} B_n)(b_{qs}^{+} + b_{qs}), \tag{4}$$

$$\chi_{qs}^{n} = A c_n^q, \qquad f_{qs}^{n} = A_{+} c_n^q, \qquad f_{qs}^{n+1} = A_{-} c_{n+1}^q,$$

$$A = D^{\phi} e_{qs}^{\phi} a_{qs}^{\phi} + D^{\psi} e_{qs}^{\psi} a_{qs}^{\psi} + D^{\xi} e_{qs}^{\xi} a_{qs}^{\xi},$$

$$A_{\pm} = M^{\psi} e_{qs}^{\psi} a_{qs}^{\psi} \pm M^{\phi} e_{qs}^{\phi} a_{qs}^{\phi},$$

where H_{ex} is the free exciton Hamiltonian; H'_{int} and H''_{int} are exciton–phonon interaction Hamiltonians. Using the canonical transformation

$$B_n = \sum_{k=1}^{N} c_n^k B_k, \qquad B_n^{+} = \sum_{k=1}^{N} c_n^k B_k^{+}, \qquad k = 1, 2, \ldots, N, \tag{5}$$

we obtain

$$H_{ex} = \sum_{k} E_k B_k^{+} B_k, \qquad E_k = \Delta E + D + 2M \cos k\vartheta,$$

$$H'_{int} + H''_{int} = \sum_{k'k''} \sum_{qs} F_{k'k''qs} (b_{qs}^{+} + b_{qs}) B_{k'}^{+} B_{k''},$$

$$F_{k'k''qs} = [2/(N+1)]^{1/2} (F_1 + F_2 + F_3),$$

$$F_1 = A(\alpha - \alpha_{+}) + (\cos \vartheta k' + \cos \vartheta k'')(\alpha_{-}\beta_{-} - \alpha_{+}\beta_{+}),$$

$$\alpha_{\pm} = (N+1)^{-1} \sin \vartheta q (\cos \vartheta(k' \pm k'') - \cos \vartheta q)^{-1} \delta_{k' \pm k'' - q, p}, \tag{6}$$

$$\beta_{\pm} = A_{+} + A_{-}(\cos \vartheta q \pm 2 \sin(\vartheta(k' - k'')/2)),$$

$$p = \pm 1, \pm 3, \ldots,$$

$$F_2 = \gamma_{+} + \gamma_{-}, \qquad \gamma_{\pm} = A_{-} \sin \vartheta q (\cos \vartheta k'' + \cos \vartheta k')/2\delta_{k' \pm q, k''} + (A_{+} + A_{-} \cos \vartheta q)(\sin \vartheta k'' \pm \sin \vartheta k')/2\delta_{k' \pm k'', q},$$

$$F_3 = (-1)^{k'+k''+q+1} 2(N+1)^{-1} \sin \vartheta q (\cos \vartheta k'' + \cos \vartheta k') \times [(A_{+} + A_{-} \cos \vartheta q) 2 \sin^2(\vartheta(k' - k'')/2) + A_{-} \cos \vartheta q \sin \vartheta k'' \sin \vartheta k'].$$

Here E_k is the energy of the kth exciton state, B_k^{+} and B_k, respectively, create and destroy the kth exciton state, and $F_{k'k''qs}$ in the interaction Hamiltonian describes the annihilation of the k''th exciton state with simultaneous creation of the k'th exciton state and the phonon of the sth branch with wave number q (at nonzero temperatures it also describes the annihilation of the k'' and qs states with the k'-state creation).

It is interesting to note that in the case of an infinite chain or a circular aggregate only terms with $k'' = k' \pm q$ are nonzero in the interaction Hamiltonian. In the case of a finite open chain the boundary conditions break the symmetry and thus disturb momentum conservation in the exciton–phonon scattering processes. That is why the scattering with arbitrary k'', k', and q is allowed. For large N the most effective exciton–phonon interactions correspond to $k' \pm k'' = q \pm 1$. For example, in the case $k'' = k' = q = 1$, the total length of the chain equals the half-period of exciton and phonon wave functions. Thus, interacting excitons and phonons are in spatial resonance. When $k'' = k' = 1$ and $q = 2$, the phonon wave function has two half-periods (positive and negative). This means that symmetric exciton states interact with the antisymmetric phonon state. The efficiency of this interaction is low ($F_1 = 0$) but is nonzero because of nonlocal exciton–phonon scattering (the $A_{\pm}$ factors involved in F_2 and F_3).

We consider low-temperature optical spectra, assuming a weak exciton–phonon coupling. In this case the perturbation theory for the Green's function developed by Davydov (1971) is valid.

The absorption spectrum of an aggregate is

$$A(\omega) = -\sum_{k} (d_k^{e})^2 \operatorname{Im}(G(k, \omega)), \qquad \mathbf{d}_k = \sum_{n=1}^{N} c_n^k \mathbf{d}_n,$$

$$G(k, \omega) = (\omega - \omega_k - M_r(k, \omega))^{-1}, \tag{7}$$

$$M_r(k, \omega) = \sum_{k'qs} F_{k'kqs}^2 (\omega - \omega_{k'} - \Omega_{qs} - M_{r-1}(k', \omega - \Omega_{qs}))^{-1},$$

where $\mathbf{d}_k$ is the transition-dipole moment of exciton level k, d_k^{e} is its projection on electric field vector $\mathbf{e}$ of the incident light, $G(k, \omega)$ is the Fourier transform of the retarded Green's function, and $M_r(k, \omega)$ is the self-energy in the rth-order approximation. In Eq. 7 $h \equiv 1$ ($E_k = \omega_k$).

Noninteracting double BChl chain models

Double-chain models are shown in Fig. 1 *B* and *C*. We consider the two-dimensional models for BChl aggregates in which the pigment–pigment interactions dominate in determining the geometrical arrangement of the pigments (a linear antiparallel double chain and a zigzag chain; see also the reviews of BChl aggregation models (Alden et al., 1992; Nozawa et al., 1994)). (The general case of a double chain is shown in Fig. 3 *E* below).

The Hamiltonian of a double chain can be written as

$$H = \sum_{n=1}^{N} (\Delta E + D_n) B_n^+ B_n + \sum_{n=1}^{N-1} M_{n,n+1}(B_n^+ B_{n+1} + B_{n+1}^+ B_n)$$

$$+ \sum_{m=1}^{N} (\Delta E + D_m) B_m^+ B_m + \sum_{m=1}^{N-1} M_{m,m+1}(B_m^+ B_{m+1} + B_{m+1}^+ B_m)$$

$$+ \sum_{n,m}^{N} M'_{n,m}(B_m^+ B_n + B_n^+ B_m), \qquad (8)$$

where n and m correspond to the first and second rows, respectively; $M'_{n,m}$ describes the interaction between the molecules from different rows. Note that $M'_{n,m} = M'_{n-m}$ owing to the translational symmetry.

The description of exciton–phonon interactions in a double-chain model is analogous to the description made in the previous section for a single-chain model. Here we restrict our analysis to the case of local exciton–phonon interactions with a single mode ($\Omega_{qs} = \Omega_q$); only the ψ coordinate is considered. In a double chain each exciton and librational phonon state, k and q, splits into two states, $k_\pm$ and $q_\pm$ (Davydov splitting). Introducing the corresponding creation and destruction operators:

$$D_n = D + D^\psi \psi_n,$$

$$\psi_n = \sum_q a_q^\psi c_n^q (b_{q+}^+ + b_{q+} + b_{q-}^+ + b_{q-})/\sqrt{2},$$

$$D_m = D + D^\psi \psi_m,$$

$$\psi_m = \sum_q a_q^\psi c_m^q (b_{q+}^+ + b_{q+} - b_{q-}^+ - b_{q-})/\sqrt{2}, \qquad (9)$$

$$B_n^+ = \sum_{k=1}^{N} c_n^k (B_{k+}^+ + B_{k-}^+)/\sqrt{2}, \quad B_m^+ = \sum_{k=1}^{N} c_m^k (B_{k+}^+ - B_{k-}^+)/\sqrt{2},$$

we obtain the Hamiltonian in the form

$$H_{ex} = \sum_k E_{k+} B_{k+}^+ B_{k+} + E_{k-} B_{k-}^+ B_{k-},$$

$$E_{k\pm} = \Delta E + D + 2M \cos k\vartheta \pm M',$$

$$H'_{int} = \sum_{k'k''q} F_{k'k''q}[(b_{q+}^+ + b_{q+})(B_{k+'}^+ B_{k+''} + B_{k-'}^+ B_{k-''})/\sqrt{2}$$

$$+ (b_{q-}^+ + b_{q-})(B_{k+'}^+ B_{k-''} + B_{k-'}^+ B_{k+''})/\sqrt{2}], \qquad (10)$$

$$F_{k'k''q} = [2/(N+1)]^{1/2} A(\alpha_- - \alpha_+), \qquad A = D^\psi a_q^\psi,$$

$$\alpha_\pm = (N+1)^{-1} \sin \vartheta q (\cos \vartheta(k' \pm k'')$$

$$- \cos \vartheta q)^{-1} \delta_{k' \pm k'' - q, p},$$

$$p = \pm 1, \pm 3, \ldots.$$

Here $F_{k'k''q}$ is the same as in Eq. 6 in the case $A_\pm = 0$. The M' value that characterizes the splitting between Davydov components is equal to

$$M' = \sum_j M'_j (N+1)^{-1} [\sin \vartheta kj \cot \vartheta k$$

$$+ (N + 1 - j) \cos \vartheta kj], \qquad (11)$$

$$M'_j = M'_{n-m}, \qquad j = 0, \pm 1, \ldots \pm (N-1).$$

In Eq. 11 all the interactions are taken into account. But in some cases the M' value is determined by nearest-neighbors interaction terms. For example, for the models shown in Fig. 1 *B* and *C*,

$$M' = M'_0 + M'_1 \cos \vartheta k. \qquad (12)$$

The absorption spectrum of a double chain is

$$A(\omega) = -\sum_k (d_{k+}^e)^2 \operatorname{Im}(G(k_+, \omega)) + (d_{k-}^e)^2 \operatorname{Im}(G(k_-, \omega)),$$

$$\mathbf{d}_{k\pm} = \sum_{n=1}^{N} \sum_{m=1}^{N} (c_n^k \mathbf{d}_n \pm c_m^k \mathbf{d}_m)/\sqrt{2},$$

$$G(k_\pm, \omega) = (\omega - \omega_{k\pm} - M_r(k, \omega))^{-1}, \qquad (13)$$

$$M_r(k, \omega) = \sum_{k'q} F_{k'kq}^2 / 2[(\omega - \omega_{k+'} - \Omega_q$$

$$- M_{r-1}(k', \omega - \Omega_q))^{-1}$$

$$+ (\omega - \omega_{k-'} - \Omega_q - M_{r-1}(k', \omega - \Omega_q))^{-1}].$$

Tubular models of tightly packed BChl chains

Consider the cylinder formed by L parallel linear chains, each containing N BChl molecules (Fig. 1 *D* and Fig. 3 *F* below; see also Holzwarth and Schaffner (1994)); n is the number of a molecule in a row; l is the number of a row, and $\mathbf{d}_{nl}$ is the transition-dipole moment of the nth molecule from the lth row. Exciton states are characterized by two numbers, k and κ, where k takes N integer values 1, 2, ... N and κ takes L integer values 0, ± 1, ± 2, ... There are L Davydov components, each having an exciton structure similar to that of a linear chain. The energies and dipole

moments of the (k, κ) exciton state are equal to

$$E_{k\kappa} = \Delta E + D + 2M \cos k\vartheta + 2M' \cos \kappa\Phi,$$

$$\mathbf{d}_{k\kappa} = \sum_{n=1}^{N} \sum_{l=1}^{L} c_n^k c_l^\kappa \mathbf{d}_{nl}, \qquad (14)$$

$$c_n^k = [2/(N+1)]^{1/2} \sin(\vartheta nk), \qquad \vartheta = \pi/(N+1);$$

$$c_l^\kappa = [1/L]^{1/2} \exp(i\Phi l\kappa), \qquad \Phi = 2\pi/L;$$

where M' is defined by Eq. 11, with n and m corresponding to the nearest-neighbor rows. The generalization of Eq. 13 to the case of L Davydov components is straightforward.

HOLE-BURNING SPECTRA

In this section we calculate the exciton level structure, homogeneous absorption spectra, and HBSs of chlorosomal antennae for different models of BChl aggregation, including the two limiting cases of noninteracting and tightly packed BChl chains as well as intermediate cases. New models of BChl aggregation with a low packing density are proposed.

Noninteracting single and double BChl chain models

Consider the absorption spectrum of a single chain in the first-order approximation ($r = 1$), assuming local exciton–phonon interactions with a single dispersionless librational mode ($\Omega_{qs} = \Omega$, $A = g\Omega$). Nonlocal interactions are neglected ($A_\pm = 0$). We used the parameter set $g = 0.5$, $N = 15$, $\phi = 0$, $M = -750$ cm^{-1}, $\Omega = 225$ cm^{-1}, and $\Gamma/2 = 3$ cm^{-1}, where Γ is the full width at half-maximum (FWHM) of each electron-vibronic line. The homogeneous line broadening that is due to relaxation from higher exciton level and vibronic relaxation is not taken into account so that a well-resolved vibronic structure can be obtained.

The absorption spectrum is shown in Fig. 2. The zero of energy is taken to be $(\Delta E + D)$, i.e., the energy is counted from the monomer absorption maximum. The lowest exciton state (~1500 cm^{-1} red shifted with respect to the monomer absorption maximum) has most of the total oscillator strength (81%). This is the common property of linear aggregates with the Q_y transition of a single BChl c directed approximately parallel to the long axis of an aggregate. In the case of weak exciton–phonon coupling most of the oscillator strength of the lowest exciton state corresponds to the zero-phonon line (ZPL). The resulting spectrum consists of an intense ZPL and of weak peaks corresponding to the second exciton level and additional peaks that are due to exciton–phonon scattering. When librational phonon frequency is in resonance with the two lowest exciton levels ($\Omega = \omega_2 - \omega_1$, i.e., 225 cm^{-1}), the ZPL slightly broadens, its amplitude decreases, and shorter-wavelength peaks become more pronounced (this case is shown in Fig. 2).

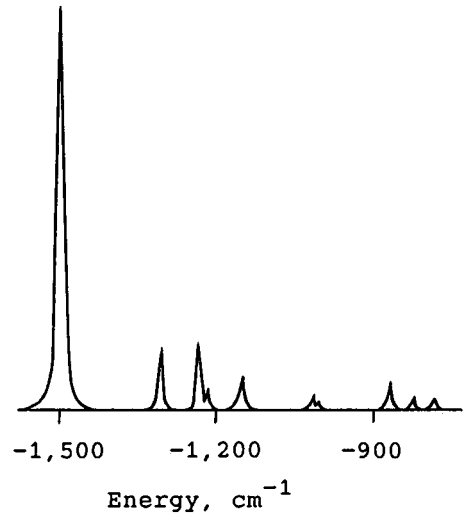

FIGURE 2 Absorption spectrum for single-chain model *A*. Line broadening is not taken into account; interaction with a single optical mode with frequency $\Omega = 225$ cm^{-1} is assumed. Other parameters are given in the text.

If the broadening of shorter-wavelength peaks is introduced, a broad wing that is blue shifted with respect to the ZPL will appear. But its integrated intensity will be much less (~19%) than that of the ZPL. This result contradicts experimental data that suggest a considerably higher intensity of the broad component (Fetisova and Mauring, 1992, 1993; Fetisova et al., 1994). That is why the single-chain models must be ruled out.

For the double-chain model (Fig. 1 *B*) $\mathbf{d}_n$ is antiparallel to $\mathbf{d}_m$ (Alden et al., 1992; Nozawa et al., 1994). Transition dipoles of molecules n and $m = n$ form a small angle with the center-to-center (Mg–Mg) line as do the transition dipoles of molecules n and $m = n + 1$. This means that $M_0' > 0$ and $M_1' > 0$ in Eq. 12. In this case $M' > 0$. From Eqs. 10 and 13 one can obtain $E_{k+} > E_{k-}$ and $(d_{k+}^e) = 0$. Actually d_{k+}^e is nonzero because of the spectral inhomogeneity of molecules in the aggregate: $(d_{k+}^e)^2/(d_{k-}^e)^2 \ll 1$. Thus, the spectrum consists of an intense ZPL corresponding to the lowest exciton level $(-k)$ and of weak shorter-wavelength peaks (as well as in the case of the single-chain models).

For the zigzag model (Fig. 1 *C*) $\mathbf{d}_n$ is almost parallel to $\mathbf{d}_m$ (Alden et al., 1992; Nozawa et al., 1994). In this case $M' < 0$ (for example, according to Alden et al. (1994) $M_0' = M_1' = -450$ cm^{-1}). In this case $E_{k+} < E_{k-}$ and $(d_{k+}^e)^2/(d_{k-}^e)^2 \gg 1$, in contrast to the case of an antiparallel chain. Now $+k$ is the lowest component, but its oscillator strength is greater than that of the blue-shifted $-$k component. Notice that the blue-shift value is $2M' = 900$ cm^{-1}.

In both cases (an antiparallel double chain and a zigzag chain), the oscillator strength of the lowest Davydov component is much greater than that of higher components. Thus, the absorption spectrum comprises the intense line corresponding to the lowest exciton level of the lowest Davydov component and weak shorter wavelength peaks;

this fact is inconsistent with results of the hole-burning experiments. Thus, the double-chain models must be ruled out as well as the single-chain models.

Tubular models of tightly packed BChl chains

If the transition dipoles of BChl molecules are parallel to the long axis of a tubular aggregate of L single chains (Fig. 1 *D*), only the $\kappa = 0$ component of the absorption spectrum is dipole allowed. We assume that $M < 0$, $M' < 0$, and the absolute values of M and M' for tightly packed BChl chains are comparable, in agreement with the assumption made by Holzwarth and Schaffner (1994). In this case the dipole-allowed $\kappa = 0$ component is the lowest among other L components. So the absorption spectrum is the same as for the single- or double-chain models. The same result arises in the case of the tubular aggregate of L double chains (see Nozawa et al., 1994). Thus, the tubular models of tightly packed BChl chains cannot explain the spectroscopic data (at least for $M' < 0$).

Notice that in the highly aggregated models of Holzwarth and Schaffner (1994) and Nozawa et al. (1994) the BChl packing density (i.e., the number of molecules/nm^2) in the tubular structures is $\rho = 1.91$ mol/nm^2 and $\rho = 1.85$ mol/nm^2, respectively, whereas the overestimated upper limit of the BChl *c* packing density in the *Chloroflexus* chlorosome (calculated following detailed analyses of chlorosome size and BChl *c* content (Golecki and Oelze, 1987; Staehelin et al., 1978)) is $\rho_h = 0.23$–0.32 mol/nm^2 for the high BChl *c* content culture. The BChl *c* packing density in the *Chlorobium* chlorosome, evaluated from the available biochemical and electron microscopy data (Olson et al., 1977; Staehelin et al., 1980), is $\rho_l = 0.32$ mol/nm^2. Thus, the overestimated upper limit of the in vivo BChl *c* packing density is 3–6 times lower than that suggested in highly aggregated models.

Alternative models with low-density packing of BChl chains

The models of noninteracting BChl chains (Smith et al., 1983; Mimuro et al., 1989; Lin et al., 1991; Alden et al., 1992) and the models with tightly packed, strongly exciton-coupled BChl chains (Holzwarth and Schaffner, 1994; Nozawa et al., 1994) correspond to the two limiting cases of BChl chain aggregation. Consider the intermediate cases. In the highly aggregated models the tubular structures contain ~20 single (Holzwarth and Schaffner, 1994) or double (Nozawa et al., 1994) BChl chains. So the model aggregate of BChl chains in the intermediate case under investigation must contain two to several exciton-coupled BChl chains (considerably fewer than 20) with the interchain distance large enough to exclude the van der Waals contacts between BChl molecules that belong to the neighboring chains.

Start with the simplest case of two exciton-coupled single chains (Fig. 3 *E*). In general, the sign of M' depends on the

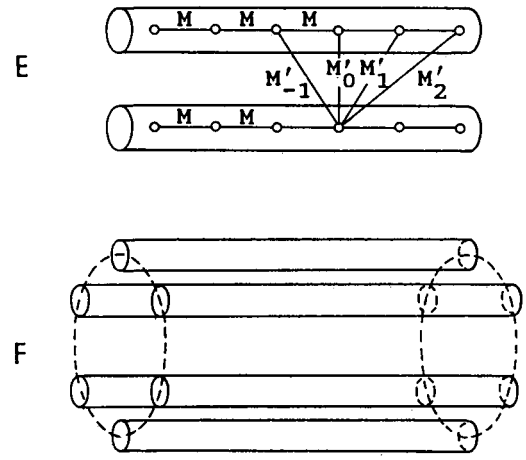

FIGURE 3 BChl aggregation models: (*E*) Two-coupled single-chain model. The equivalent schematic is shown, where M and M'_j (j = . . ., −1, 0, 1, 2, . . .) are the interaction energies between the corresponding BChls (treated as point dipoles and shown by small circles). (*F*) Tubular model with a low density of coupled BChl chain packing.

interchain distance. For example, for an antiparallel double chain the sign of M' changes from positive to negative when the distance between chains increases. For $M' < 0$ the lowest Davydov component has a low intensity, in contrast with the case $M' > 0$, when the intensity of the lowest component is much greater than the intensities of higher components.

To explain hole-burning data we must assume that $M' < 0$ for antiparallel chains (or $M' > 0$ for parallel chains), i.e., a large interchain distance.

On the other hand, the double-chain model with a large interchain distance allows one to explain the small value of the energy gap between Davydov components that is due to a small M' value. The M' value must be approximately 100–200 cm^{-1} to explain the 200–400-cm^{-1} energy gap between the ZPH and the broad hole maximum (Fetisova and Mauring, 1992, 1993; Fetisova et al., 1994). The 100–200-cm^{-1} interaction energy corresponds to the interchain distance of 1.6–2.0 nm. Hence, direct pigment–pigment contacts between different chains are improbable. One can assume that the spatial organization of two such chains, as well as the assembly of several such pairs of chains into a tubular structure, can be determined by the pigment–protein interaction (Lehmann et al., 1994) or by another type of interaction: for example, the interaction of pigments with the hypothetical liquid-crystal matrix, which, we believe, is the case for the in vivo chlorosome.

The absorption spectrum for the model of Fig. 3 *E* is shown in Fig. 4. We used the first-order approximation ($r = 1$), the single-mode limit ($\Omega_{qs} = \Omega$) and the following parameters: $g = 0.5$, $N = 8$, $M = -750$ cm^{-1}, $M' = 150$ cm^{-1}, $\Omega = 300$ cm^{-1}, $\Gamma/2 = 3$ cm^{-1}, and the ratio of oscillator strengths of Davydov components $(d^e_{k+})^2/(d^e_{k-})^2 = 10$.

The spectrum consists of lines centered at −1300 cm^{-1} (the strongest) and −550 cm^{-1}, corresponding to the most

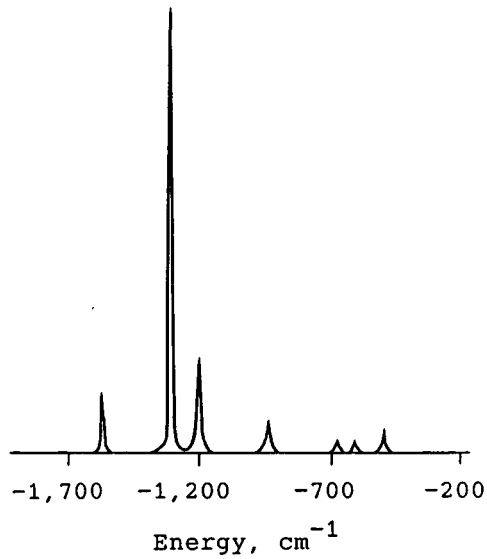

FIGURE 4 Absorption spectrum for two coupled single-chains model *D*. The phonon frequency is $\Omega = 300$ cm^{-1}. Other parameters are given in the text.

intense Davydov component ($k_+ = 1$ and $k_+ = 3$ levels). The line at -1550 cm^{-1} corresponds to the second Davydov component (the $k_- = 1$ level). There are additional peaks that result from exciton–phonon scattering.

The -1550-, -1300-, and -550-cm^{-1} lines correspond to the ZPH, the broad-hole maximum, and the short-wavelength wing, respectively, of the HBS. On the other hand, for all green bacteria investigated the positions of the ZPH and the broad-hole maximum closely correspond to the positions of the two lowest components of the circular dichroism (CD) spectrum (Fig. 5 *D*; Fetisova et al., 1995). So we may conclude that the -1550-, -1300-, and -550-cm^{-1} exciton levels correspond to the three components revealed by CD spectra (Fig. 5). The splitting between two lowest exciton levels is proportional to M' and can exhibit some variation for different bacteria (because M' takes values from 100 to 200 cm^{-1} (Fetisova et al., 1995)).

Notice that the energy gap between the $k_+ = 1$ and the $k_+ = 3$ levels is $E_3 - E_1 = -2M(\cos 3\vartheta - \cos \vartheta)$ and depends only on the N value, because M is determined by the red shift value. For $M = -750$ cm^{-1} we obtain $N = 7$–9 to explain the experimentally observed energy gap between E_3 and E_1.

When the librational phonon frequency is in resonance with the $k_+ = 1$ and $k_- = 1$ levels ($\Omega = \omega_{k+} - \omega_{k-}$, i.e., 300 cm^{-1}) significant changes in the spectrum occur near the $k_+ = 1$ and $k_+ = 3$ lines (this case is shown in Fig. 4). In particular, the amplitude of the $k_+ = 1$ line (-1300 cm^{-1}) decreases, and the satellite phonon peaks (at -1200, -950, and -600 cm^{-1}) become more pronounced.

The models of two exciton-coupled double and zigzag chains were analyzed as well. Their spectral properties are very similar to those of two exciton-coupled linear chains.

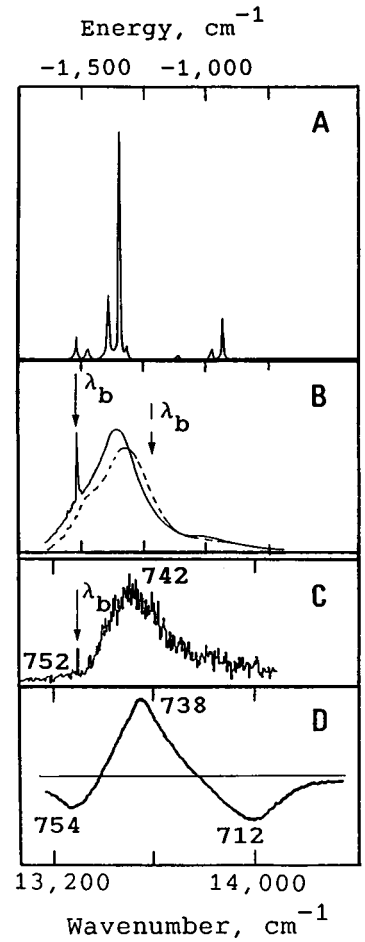

FIGURE 5 Spectra for six-coupled-chains model *E*. (*A*) Calculated low-temperature absorption spectrum with $\Omega = 30$ cm^{-1} and homogeneous linewidth $\Gamma/2 = 2$ cm^{-1}. (*B*) Calculated HBS for the same conditions after introduction of the 180-cm^{-1} homogeneous linewidth (FWHM) for higher levels and the 90-cm^{-1} inhomogeneous width (FWHM). (*C*) Experimental HBS (the ordinate axis is in arbitrary units) for intact cells of *C. aurantiacus* at 1.8 K. The burning wavelength (λ_b) corresponds to the maximum of the lowest exciton level absorption band of BChl *c* (752 nm). (*D*) Experimental CD spectrum (the ordinate axis is in arbitrary units) of intact cells of *C. aurantiacus* at room temperature. Two energy scales are shown, corresponding to the energy counted from the monomer absorption maximum (*upper scale*, for theoretical spectra *A* and *B*) and to the absolute wave numbers (*lower scale*, for experimental spectra *C* and *D*).

We calculated the absorption spectrum shown in Fig. 4 without taking into account the homogeneous broadening of higher exciton levels that is due to relaxation to the lowest exciton level. If the homogeneous broadening of the shorter-wavelength peaks of the spectrum shown in Fig. 4 is introduced, the very intensive broad wing that is blue shifted with respect to the $k_- = 1$ origin line appears (not shown). This broad wing corresponds to the experimental broad featureless nonresonant hole. To fit an experimental spectrum for *C. aurantiacus* (Fetisova and Mauring, 1992) one must assume a 200-cm^{-1} homogeneous width (FWHM) for higher exciton levels. The corresponding time constant of exciton relaxation is ~50 fs. Notice that fast energy equil-

ibration with the 50–100-fs time constant (or even <50 fs) was observed in recent femtosecond pump–probe experiments (Savikhin et al., 1994, 1995).

We conclude that the model of two exciton-coupled chains gives a reasonable interpretation of the experimentally observed HBS. Assembling three or four such pairs of chains into a tubular structure 5–10 nm in diameter in principle models the rod element with optical properties appropriate to the chlorosome. However, according to the data on supramolecular organization of chlorosomes (Staehelin et al., 1978, 1980) the BChl *c*, *d*, or *e* pigments are thought to be associated with six subunits organized hexagonally in rods running the length of each chlorosome. Logically, we can assume that there is at least one linear (single or double) BChl chain/subunit, i.e., six such chains/rod. On the other hand, the in vivo BChl packing density values are compatible with no more than one such (continuous) chain/rod subunit. Besides, to explain the spectral features revealed by hole-burning experiments (Fetisova and Mauring, 1992, 1993; Fetisova et al., 1994, 1995) in the framework of a tubular model, we must assume that M is ~ -750 cm^{-1} and that M' is approximately 50–100 cm^{-1}. In this case the energy gap between the dipole-allowed $\kappa = 0$ level and the lowest $\kappa = L/2$ level (weakly nonforbidden because of site inhomogeneity) is $4M' = 200-400$ cm^{-1}. The 50–100-cm^{-1} interaction energy corresponds to an interchain distance of 2 nm or more. This strongly suggests that the spatial organization of L chains into a tubular structure cannot be determined by self-aggregation of pigments into an entire macrocycle network, as was postulated by Holzwarth and Schaffner (1994) and by Nozawa et al. (1994). Besides, the interchain distance of ~2 nm imposes strict limitations on the maximum possible L value: the model rod element may contain no more than six single or double chains ($L = 6$), each arranged as proposed by Holzwarth and Schaffner (1994) or by Nozawa et al. (1994). Thus, the most realistic models of natural rods are the tubular models with no more than six (single or double) exciton-coupled linear BChl chains.

Consider this tubular model with $L = 6$ (Fig. 3 *F*). The absorption spectrum for $\Omega = 30$ cm^{-1}, $N = 10$, $M = -750$ cm^{-1}, $M' = 45$ cm^{-1}, and $\Gamma/2 = 2$ cm^{-1} is shown in Fig. 5 *A*. The relative intensities of Davydov components $\kappa = 0$, $\kappa = \pm 1$, $\kappa = \pm 2$, and $\kappa = 3$ are 100, 27, 3, and 1.6, respectively. The $\kappa = \pm 1$, $\kappa = \pm 2$, and $\kappa = 3$ components are assumed to be weakly nonforbidden because of site inhomogeneity; the corresponding intensities are proportional to the square of their displacement from the dipole-allowed $\kappa = 0$ state. The $k = 1$ levels of the $\kappa = 0$, $\kappa = \pm 1$, $\kappa = \pm 2$, and $\kappa = 3$ components correspond to the −1370-, −1415-, −1505-, and −1550-cm^{-1} lines, respectively (Fig. 5 *A*). The $k = 3$ levels of the $\kappa = 0$ and $\kappa = \pm 1$ components correspond to the −950- and −995-cm^{-1} lines, respectively (Fig. 5 *A*).

The −1550-cm^{-1} line corresponds to the ZPH of the HBS and to the lowest component of CD spectrum; the −1370- and −950-cm^{-1} lines correspond to the two higher (blue-shifted) components of CD spectrum; the most intense −1370-cm^{-1} line also corresponds to the broad-hole maximum of the HBS (Fig. 5 *A–D*).

To calculate the HBSs we must take into account inhomogeneous line broadening that is due to diagonal energy disorder (the nonidentity of ΔE for individual BChls in an aggregate) and to the nonidentity of different aggregates (the variation of ΔE from aggregate to aggregate without any dispersion of ΔE within an aggregate). Here we take into account only the second type of inhomogeneous broadening. In this case the inhomogeneous broadening can be described by the Gauss distribution $W(E_k)$ of energies E_k with a width Γ_{inh}.

The hole-burning spectrum can be calculated from the following expression (Friedrich and Haarer, 1984):

$$\Delta A(\omega) = \int dE_k A(\omega - E_k) W(E_k) (\exp(-CA(\omega_B - E_k)) - 1), \tag{15}$$

where ω_B is the burning frequency, C is a constant that depends on the burning time and the photon flux, and $A(\omega - E_k)$ is given by Eq. 7 or 13.

We introduced the 180-cm^{-1} homogeneous line width (FWHM) for all the exciton levels (except for the lowest ($k = 1$, $\kappa = 3$) level) and the inhomogeneous width $\Gamma_{inh} = 90$ cm^{-1} (FWHM). The hole profiles are shown in Fig. 5 *B* for the $CA(\omega) \ll 1$ limit. Arrows show the burning frequencies. The sharp ZPH can be burned only when the burning frequency corresponds to the long-wave side of the spectrum. When the burning frequency corresponds to the short-wave side, a broad HBS without a ZPH is produced.

Thus, the tubular model of six coupled BChl chains is in good agreement with the experimental HBS. In particular, the energy gap between a ZPH and a broad nonresonant hole, their relative intensities, and the large width of a nonresonant hole (Fig. 5 *A–D*) can be explained if we assume reasonable values of interaction energies and interchain distances.

We suggest that the BChl–BChl interactions dominate only in determining the BChl chain structure. The spatial arrangement of the chains into tubular structures, with the interchain distance of ~2 nm predicted by our theory from experimental HBSs, is however assumed to involve another type of interaction, for example, those typical of liquid crystals. Indeed, liquid crystals are unique systems that exhibit both a molecular mobility and an orderly structure, which are integral features of living systems. Aligned molecules of a liquid crystal form an ideal medium for optimal functioning of biological structures, particularly for efficient energy transfer in photosynthetic antennae (Fetisova, 1994). The long-range molecular order of the main light-harvesting pigments in chlorosomes in situ discovered by us (Fetisova et al., 1988) allows one to assume that the chlorosome is a biological liquid crystal. It is well known that porphyrines, many proteins, nucleic acids, hemes, lipids, and polysaccarides as well as many detergents form stable

liquid-crystalline structures in aqueous media. That is why many BChl *c/d/e* systems in vitro are essentially of a liquid crystalline nature. It is very important that liquid crystals display polymorphism; i.e., they may exist in several liquid-crystalline phases. Polymorphism is due to the response of liquid crystals to the external effects, for example, to the change in the chemical composition of the medium (i.e., the liquid crystals possess properties of living systems). Thus, a suitable medium allows one to find many different in vitro systems that resemble those in vivo with similar absorption spectra. At the same time, liquid crystals have unique structures: rods (resembling the chlorosomal ones!), cones, parallel flat layers, etc., which are typical of a liquid crystal as a whole only; possibly that is why the rod element of the chlorosome had not been isolated. It is the properties listed above that are indispensable for the level of organization that is intermediate between the organization of the continuous medium (liquid or crystalline body) and that of a living cell.

THEORY OF EXCITATION ENERGY TRANSFER BETWEEN AGGREGATES

General

Consider some basic equations for the rate constant corresponding to the excitation transfer between clusters A and A'. We assume that the A and A' clusters consist of N and N' strongly interacting pigment molecules ($N \geq 1, N' \geq 1$). The interaction of molecules n and m (where n and m are the molecule numbers in the clusters), which belong to different clusters, is weak.

Consider the energy transfer rate between two isolated molecules n and m (Forster, 1965):

$$K_n^m = f_n^m W_n^m p_n, \qquad W_n^m = |\langle m|\hat{M}|n\rangle|^2, \tag{16}$$

where f_n^m is Forster's overlapping integral for the $n \rightarrow m$ transfer, p_n is the excitation population probability for molecule n, W_n^m is the matrix element of interaction operator $\hat{M}$, and $|n\rangle$ is the state when the nth molecule is excited. According to Forster's theory, the dipole–dipole transfer occurs only if the $|n\rangle$ and $|m\rangle$ states are dipole allowed. Equation 16 can be generalized if the interaction of molecule m with cluster A is considered. The latter is characterized by a set of exciton states $|k\rangle$ with energies E_k. For the rate constant of the $A \rightarrow m$ transfer we can write

$$K_A^m = \sum_k f_k^m W_k^m p_k, \qquad W_k^m = |\langle m|\hat{M}|k\rangle|^2. \tag{17}$$

The rate of the backtransfer $m \rightarrow A$ is

$$K_m^A = \sum_k f_m^k W_m^k, \qquad W_m^k = |\langle k|\hat{M}|m\rangle|^2, \tag{18}$$

where p_k is the population probability for excitonic level $|k\rangle$ and f_k^m and f_m^k are the overlapping integrals, i.e., Frank–Condon overlapping factors between phonon states associated with the $|m\rangle$ and $|k\rangle$ levels averaged over the initial state. We assume fast vibrational relaxation (this is the basic assumption of Forster's theory) as well as fast thermalization of exciton-state population. Notice that because of the fast relaxation of the higher exciton levels the f_k^m factors corresponding to the lowest k level and to the higher levels are rather different. It is very important that the W_k^m factors for the $|k\rangle \rightarrow |m\rangle$ transfer can be nonzero, even in the case of dipole-forbidden $|k\rangle$ states. For example, any $|k\rangle$ state can be dipole forbidden because of the spatial symmetry of its wave function, but this symmetry will have no effect on the matrix element in W_k^m if molecule m interacts only with a small number of molecules from aggregate A (see below). That is why there is no correspondence between the rate constant K_A^m and the overlapping of fluorescence and absorption spectra of a donor and an acceptor, as in the case of the monomer $\rightarrow$ monomer transfer.

Similarly, the rate of EET from cluster A to cluster A' is

$$K_A^{A'} = \sum_{k,k'} f_k^{k'} W_k^{k'} p_k, \qquad W_k^{k'} = |\langle k'|\hat{M}|k\rangle|^2. \tag{19}$$

In general, exciton wave functions $|k\rangle$ and $|k'\rangle$ are linear combinations of wave functions $|n\rangle$ and $|m\rangle$, corresponding to molecules n and m from different aggregates. This means that matrix element $\langle k'|\hat{M}|k\rangle$ can be represented as a linear combination of $M_{nm} = \langle m|\hat{M}|n\rangle$, where

$$M_{nm} = R_{nm}^{-3}(\mathbf{d}_n \cdot \mathbf{d}_m - 3(\mathbf{d}_n \cdot \mathbf{e}_{nm})(\mathbf{d}_m \cdot \mathbf{e}_{nm})), \tag{20}$$

where R_{nm} is the distance between molecules n and m from different aggregates, $\mathbf{d}_n$ and $\mathbf{d}_m$ are the transition-dipole moments of these molecules, and $\mathbf{e}_{nm}$ is the unit vector directed from one molecule to the other.

Similarly, elements $\langle m|\hat{M}|k\rangle$ and $\langle k|\hat{M}|m\rangle$ in Eqs. 17 and 18 are linear combinations of M_{nm}, where molecule n belongs to the aggregate and m is an isolated molecule (trap).

Excitation energy transfer between linear chains

If clusters A and A' have the form of linear aggregates, each containing N identical molecules with C_N symmetry, then exciton states $|k\rangle$ can be expressed as

$$|k\rangle = (2/(1+N))^{1/2} \sum_{n=1}^{N} \sin(k\vartheta n)|n\rangle. \tag{21}$$

The matrix elements in Eqs. 17–19 take the following form:

$$W_k^m = 2/(1+N)\left|\sum_{n=1}^{N} M_{nm}\sin(k\vartheta n)\right|^2, \qquad W_k^m = W_m^k, \tag{22}$$

$$W_k^{k'} = 4/(1+N)^2\left|\sum_{n}^{N}\sum_{m}^{N} M_{nm}\sin(k\vartheta n)\sin(k'\vartheta m)\right|^2. \tag{23}$$

It is convenient to replace values M_{nm}, f_k^m, and $f_k^{k'}$ in Eqs. 15–20, 22, and 23 by their dimensionless forms $\bar{M}_{nm}$, $\bar{f}_k^m$, and $\bar{f}_k^{k'}$, respectively. To obtain $\bar{M}_{nm}$ it is essential, first, to normalize R_{nm} to critical distance R_0 (Forster's radius) for an isoenergetic monomer–monomer transfer and, second, to normalize $\mathbf{d}_n$ to its absolute value d. As a result we obtain $\bar{M}_{nm} = (R_0/R_{nm})^3 K_{nm}$, where K_{nm} is the orientation factor ($0 \le K_{nm}^2 \le 4$). The $\bar{f}_k^m$ and $\bar{f}_k^{k'}$ values are overlapping integrals f_k^m and $f_k^{k'}$ normalized to the overlapping integral for a transition between two identical monomers. Using the $\bar{M}_{nm}$, $\bar{f}_k^m$, and $\bar{f}_k^{k'}$ values in Eqn. 17–19, 22, and 23, we obtain the rate constants expressed in units of $(\tau_0)^{-1}$, where τ_0 is the radiation lifetime of a monomer molecule.

To discuss the physical principles of energy transfer between linear aggregates we rewrite Eqs. 22 and 23 in a simplified form:

$$W_k^m = 2M_{eff}^2 N_{eff}^2/(1 + N), \tag{24}$$

$$W_k^{k'} = 4M_{eff}^2 N_{eff}^2 N^2/(1 + N)^2, \tag{25}$$

where N_{eff} is the effective number of monomers in an aggregate interacting with a separate molecule from another BChl c aggregate or with a single BChl a molecule (trap); M_{eff} is the interaction energy averaged over this effective area.

Notice that the rate constant for energy transfer of a localized excitation from a linear chain to a trap or between two chains is given by Eqs. 24 and 25 with N_{eff}^2 replaced by N_{eff}. Thus, the strong coupling within a linear chain increases the energy transfer rate by a factor of N_{eff} (Fetisova et al., 1989).

For a small aggregate, N_{eff} is equal to N, and the efficiency of energy transfer increases rapidly with increasing N (Eqs. 24 and 25). However, if N becomes larger than N_{eff}, then N_{eff} = constant in Eqs. 10 and 11, and the further increase in aggregate size N does not accelerate the energy transfer process. A more detailed study of Eqs. 22 and 23 shows that the optimal aggregate size can be even less than the effective interaction area N_{eff} because of orientation factor K_{nm}. For simplicity we assume that the BChl c transition-dipole moments are strictly parallel to the long axis of the aggregate and that the BChl a transition-dipole moments are parallel to the BChl c transition dipoles. In this case K_{nm} is positive for $|n - m| < N_{cr}/2$ and negative for $|n - m| > N_{cr}/2$, where $N_{cr} = 1 + \sqrt{2}(R'/R)$; R is the BChl–BChl distance within the aggregate; R' is the interchain distance (or the distance between the BChl chain and a trap). It can be shown that W_k^m and $W_k^{k'}$ have maxima when $k = N/N_{cr}$ and $k = k' = N/N_{cr}$, where $k = 1, 2, \ldots$ is the exciton state number. (In this case changes in the sign of K_{nm} coincide with changes in the sign of exciton wave functions.) Thus, optimal aggregate size N is equal to N_{cr}, $2N_{cr}$, $3N_{cr}$ .... N must be slightly less than kN_{cr} if one takes into account the nonuniform shape of the exciton wave function. Notice that linear losses (radiative and nonradiative) of an aggregate increase with increasing N. That is why the case of $N = N_{cr}$ is most preferable. For example, for $R' = 3.3$ nm and $R = 0.7$ nm the N_{cr} value is $N_{cr} = 8$ and corresponds to the 5.6-nm area that is close to the period of the baseplate structure (~6 nm). This situation is extremely favorable for optimization of the energy transfer process.

Excitation energy transfer between tubular aggregates

Exciton states $|k, \kappa\rangle$ of a tubular aggregate formed by L linear rows, each containing N molecules, can be expressed as

$$|k, \kappa\rangle = \left(\frac{2}{L(1 + N)}\right)^{1/2} \sum_{n=1}^{N} \sum_{l=1}^{L} \exp(i\Phi l\kappa)\sin(k\vartheta n)|n, l\rangle. \tag{26}$$

The matrix elements of energy transfer from the $|k, \kappa\rangle$ state to trap m or to the $|k', \kappa'\rangle$ state corresponding to another aggregate take the following form:

$$W_{k\kappa}^m = \frac{2}{L(1 + N)}\left|\sum_{n,l} M_{nl,m} \exp(i\Phi l\kappa)\sin(k\vartheta n)\right|^2 \tag{27}$$

$$W_{k\kappa}^{k'\kappa'} = \frac{4}{L^2(1 + N)^2}\left|\sum_{n,l,m,l'}\sum M_{nl,ml'} \exp(i\Phi l\kappa - i\Phi l'\kappa')\sin(k\vartheta n)\sin(k'\vartheta m)\right|^2. \tag{28}$$

The energy transfer between tubular aggregates is determined by the interaction between nearest chains (two or three chains from each tubular aggregate). The contribution from each interacting pair of chains (the lth chain from one aggregate and the l'th chain from another aggregate) is proportional to $\exp(i\Phi l\kappa - i\Phi l'\kappa')$. The most effective transfer occurs between the $\kappa = 0$ and $\kappa' = 0$ components. In contrast, the rate of energy transfer between the lowest components $\kappa = L/2$ and $\kappa' = L/2$ that are proportional to $\Sigma(-1)^{l-l'}$ is near zero. This fact should result in a decrease in energy transfer rate at low temperatures.

In the case of tubular aggregates there is an optimal chain size N, as in the case of isolated chains interaction. One can determine the N_{cr} value corresponding to the interaction between each pair of chains l and l' or between each chain l and molecule m (trap). This N_{cr} value must be averaged over those chains that give the main contribution to the sum in Eq. 28 to yield the optimal N value.

Excitation energy transfer within the chlorosome

We used the supramolecular three-dimensional model of the chlorosome proposed by Staehelin et al. (1978). The chlorosome contains p layers of rod elements (Fig. 6; in the figure $p = 3$) packed into a hexagonal structure. Each rod element consists of tubular aggregates of six exciton-cou-

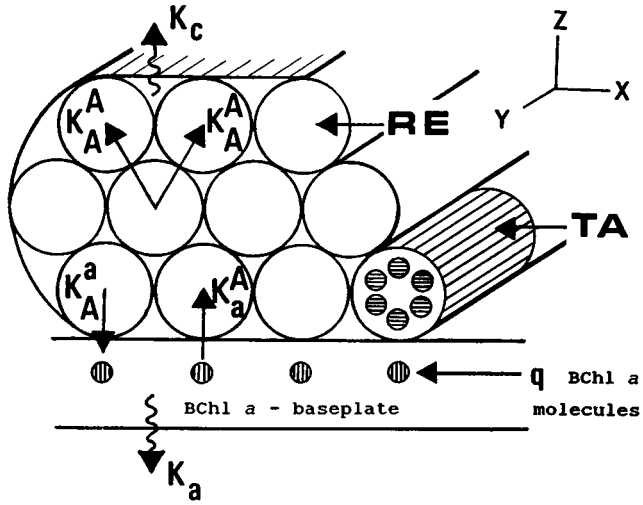

FIGURE 6 Chlorosome model. Rod elements (*RE*) are packed in a hexagonal structure. In this figure the number of rod elements layers $p = 3$. Each rod element consists of tubular aggregates (*TA*) of six BChl *c* chains described above (see model *F* in Fig. 3). Each tubular aggregate interacts with q BChl *a* molecules of the baseplate. Other symbols are defined in the text.

pled BChl *c* chains described above. We assume that the distances between nearest chains from neighboring aggregates are large enough that we can consider Forster's type of energy transfer between the aggregates.

Each aggregate from the first layer (nearest to the baseplate) interacts with q BChl *a* (BChl790) molecules of the baseplate. The rate constant of energy transfer from an aggregate of the pth layer to each of the two nearest aggregates of the $(p + 1)$st layer is K_A^A; the rate of energy transfer from the BChl *c* tubular aggregate to the BChl790 molecule of the baseplate is K_A^a; the rate of backtransfer is K_a^A. The rates of the total losses in chlorosomal BChl *c* and BChl *a* antennae are K_c and K_a, respectively (Fig. 6).

We assume that the antenna is infinite in the x and y directions to consider the one-dimensional energy migration along the z axis, because the efficiency of the BChl *c* → BChl *a* energy transfer is determined by the efficiency of energy migration only along this axis (Fig. 6) and hence only by one chlorosome size, namely, by its height and, as a consequence, by the number of rod element layers.

We obtained the analytical expression for the time constant of the fluorescence decay in the BChl *c* antenna as a function of the number of rod layers, p. The quantum yields of the losses in the BChl *c* antenna, containing p layers of rod elements, and in the baseplate BChl790 antenna, $\Phi_c(p)$ and $\Phi_a(p)$, are

$$\Phi_a(1) = \frac{t^+}{(1 + t^+ + t^-)}, \qquad p = 1,$$

$$\Phi_a(p) = \frac{(t^+/p)B_p}{(1 + t^+ + t^- + t(1 + t^-))D_{p-1} + t^2(1+t^-)D_{p-2}}, \qquad p>1,$$

$$D_0 = 1, \qquad D_1 = -(1 + t), \qquad B_1 = 1, \tag{29}$$

$$D_p = -(1 + 2t)D_{p-1} - t^2 D_{p-2},$$

$$B_p = D_{p-1} - tB_{p-1}, \qquad p > 1,$$

$$t = 2K_A^A/K_c, \qquad t^+ = qK_A^a/K_c, \qquad t^- = K_a^A/K_a,$$

$$\Phi_c = 1 - \Phi_a.$$

The time constant of the fluorescence decay in the BChl *c* antenna is

$$\tau(p) = (1 - \Phi_a(p))\tau_c, \qquad \tau_c = 1/K_c. \tag{30}$$

As is known, the chlorosomal BChl *c* antenna size depends on growing conditions (Golecki and Oelze, 1987). One may expect that all sizes of chlorosomes (including that in the z direction, i.e., the height of the chlorosome) in any cell culture will be variable over some range. Then the cells containing chlorosomes of different sizes can be characterized by the discrete distribution function $F(p)$, where $F(p)$ is the relative number of chlorosomes with p layers. In this case the time constant of the fluorescence decay in the BChl *c* antenna is

$$\tau = \sum_p \tau(p)F(p). \tag{31}$$

If the $\tau(p)$ dependence is linear, then

$$\tau = \tau(\langle p \rangle), \qquad \langle p \rangle = \sum_p pF(p). \tag{32}$$

EXCITATION ENERGY TRANSFER DYNAMICS IN THE GREEN BACTERIUM *CHLOROFLEXUS AURANTIACUS*

All experiments were performed on intact cells of the filamentous nonsulfur thermophilic green bacterium *Chloroflexus aurantiacus* strain Ok-70-fl (collection of Leiden University, Leiden, The Netherlands) used in their own growth medium under strictly anaerobic conditions. In our experiments several *Chloroflexus aurantiacus* cultures with different BChl *c* content were used (Golecki and Oelze, 1987; Oelze, 1992). We adjusted the different sizes of the chlorosomal antennae (i.e., the different ratios of BChl *c*/BChl *a*) by changing the cell growth rate (Oelze and Fuller, 1987) and by inhibiting the formation of BChl *c* with gabaculine used in different concentrations according to Oelze (1992). 0.7-, 1.6-, and 2.2-μM gabaculine concentrations were used.

We examined four cultures of *C. aurantiacus* cells with different BChl *c* content, as seen from the absorption spectra normalized at the wavelength of the membrane BChl *a* absorption maximum (~865 nm) shown in Fig. 7.

It should be stressed that the efficiency of EET from the three-dimensional chlorosomal BChl *c* antenna to the BChl *a* antenna of the baseplate is determined only by one chlorosome dimension, namely, by its height, and hence as a

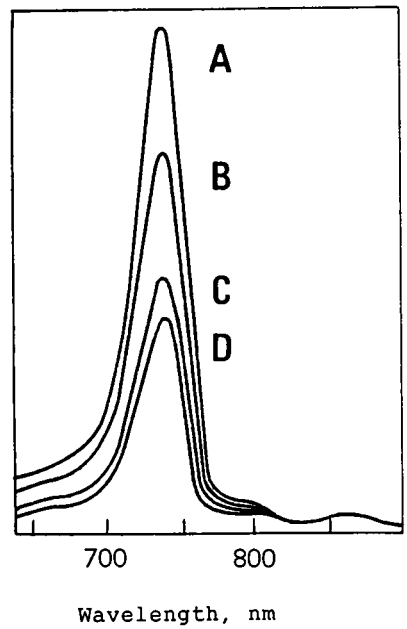

FIGURE 7 Room-temperature near-infrared absorption spectra of intact cells of four *C. aurantiacus* cultures (*A–D*) with different BChl *c* content, grown at the following concentrations of gabaculine: (*A*) 0 μM, (*B*) 0.7 μM, (*C*) 1.6 μM, (*D*) 2.2 μM. The absorption maximum at 740 nm belongs to BChl *c* of the chlorosome; the absorption maxima at ~800 and ~865 nm belong to BChl *a*.

consequence by the number of rod layers (see Fig. 6). That is why electron microscopy studies of cells under investigation were undertaken.

For electron microscopic examination the cells were fixed in the culture medium at 55°C by glutaraldehyde, postfixed with OsO_4, embedded in Epon-812, and ultrathin sectioned by standard methods (Staehelin et al., 1978). Micrographs of the ultrathin sections were used for morphometric measurements to yield histograms of chlorosome heights for the four cell cultures under investigation. The number of layers of rod elements in a chlorosome was calculated on the assumption that the diameter of each rod element was 5.5 nm (Staehelin et al., 1978; Sprague et al., 1981).

We discovered that in each culture (and even in one and the same cell!) there are chlorosomes with different numbers of rod layers. It was shown that the cells from each culture can be characterized by their own discrete distribution functions $F(p)$, where $F(p)$ is the relative number of chlorosomes with p layers. The corresponding distribution functions $F(p)$ for the four cultures under study (*A–D*) are shown in Fig. 8. In line with the results obtained by Golecki and Oelze (1987), we have shown that cells with a higher BChl *c* content (see Fig. 7) exhibit a larger number of thicker chlorosomes (compare $F(p)$ distributions for different cultures).

To investigate the antenna-size-dependent exciton dynamics within the entire chlorosome we used picosecond fluorescence spectroscopy because it could be applied to

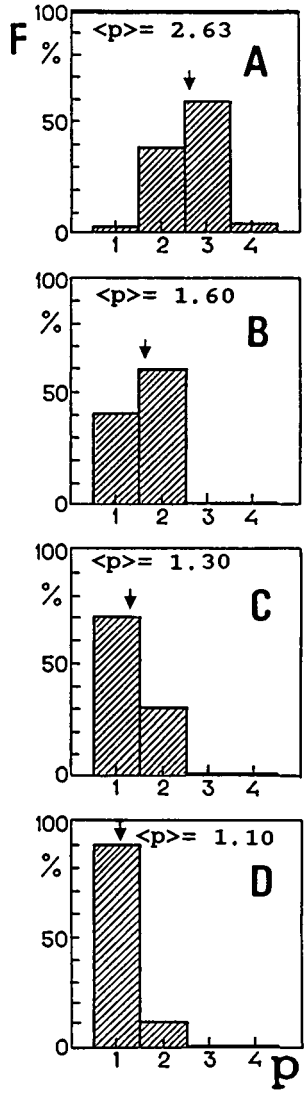

FIGURE 8 Discrete distribution function $F(p)$, where F is the number of chlorosomes with different numbers of rod elements layers (p) for each of the four *C. aurantiacus* cultures (*A–D*) shown in Fig. 7. $\langle p \rangle$ is the mean value of p calculated for each culture.

photosynthetic material in situ. The picosecond BChl *c* and BChl *a* fluorescence kinetics detected at wavelengths of the corresponding fluorescence maxima, 750 and 880 nm, respectively, were measured in intact cells for the same cultures of Figs. 7 and 8 at room temperature. The kinetics observed were unchanged over an approximately 10^3-fold decrease in the laser pulse intensity. Thus under our excitation conditions (0.2 W/cm^2) neither singlet–singlet nor singlet-triplet annihilation took place. Figs. 9 and 10 show the picosecond isotropic fluorescence decay kinetics for BChl *c* and BChl *a* emissions, respectively, in living cells of the four cultures under investigation, *A–D* (shown also in Figs. 7 and 8). All kinetics for BChl *c* emission are strongly biphasic and characterized by a fast phase with a lifetime τ_f = 40, 21, 17, and 12 ps for cultures *A*, *B*, *C*, and *D*, respectively, and a slow phase with a lifetime τ_s = 200–250

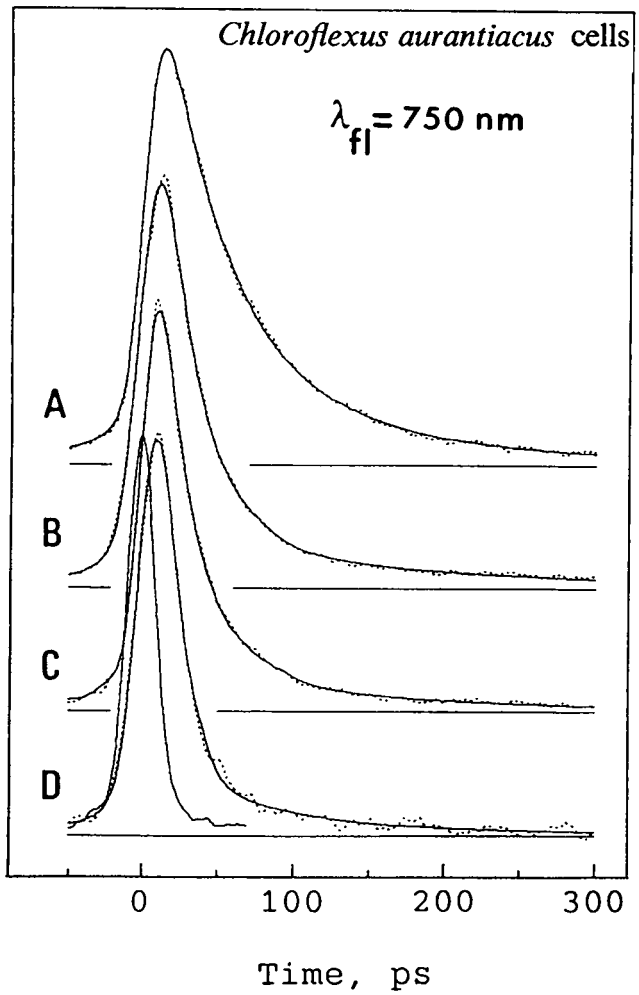

FIGURE 9 Room-temperature isotropic picosecond fluorescence kinetics for BChl *c* (at 750 nm) fluorescence decay (*dotted curves*) in living cells for each of the four *C. aurantiacus* cultures (*A–D*) shown in Figs. 7 and 8. The solid curves are the best multiexponential fits to the data (within an accuracy of 5%). Excitation was at 590 nm. The narrow profile (FWHM = 10 ps) is the apparatus response function.

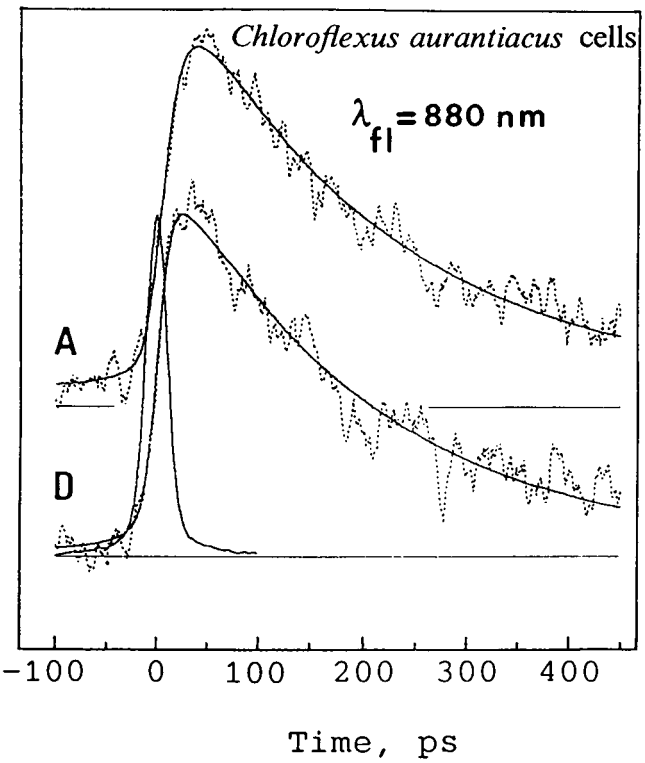

FIGURE 10 Room-temperature isotropic picosecond fluorescence kinetics for BChl *a* (at 880 nm) fluorescence decay (*dotted curves*) in living cells for two *C. aurantiacus* cultures (*A* and *D*) shown in Figs. 7–9. The solid curves are the best multiexponential fits to the data (within an accuracy of 15%). The narrow profile is the apparatus response function.

ps for all cultures (the amplitude ratio $A_f/A_s \sim 15$). All kinetics for BChl *a* emission are monophasic, with a lifetime of ~200 ps for all cultures *A–D* (in Fig. 10 only the kinetics for cultures *A* and *D* are shown).

As should be expected, each culture is characterized by its own antenna-size-dependent time constant of fluorescence decay in the BChl *c* chlorosomal antenna. Thus, the efficiency of energy transfer from the BChl *c* antenna to the baseplate BChl *a* antenna (and, hence, the rate constant of fluorescence decay in the BChl *c* antenna) decreases with increasing chlorosome size (i.e., the number of rod layers). That is why the published values of BChl *c* fluorescence decays in whole cells exhibit lifetimes in a rather wide range, from ~15 to 40 ps (Fetisova et al., 1988; Mimuro et al., 1989; Causgrove et al., 1990; this work).

The membrane BChl *a* antenna size (the number of BChl *a* molecules per reaction center) remains unchanged (Olson, 1980) for all cultures investigated. That is why the BChl *a* fluorescence kinetics are unchanged also.

It should be stressed that in any real object under investigation (for example, in cells of culture *A*) we can register only the results of a simultaneous functioning of chlorosomal antennas that differ in their size and consequently in times of BChl *c* fluorescence decay (for instance, up to four times in culture *A*; see Fig. 8). Probably this fact made researchers suggest the existence of more than one pool of antenna pigments (two pools at least in *C. aurantiacus* chlorosomes). Meanwhile, the HBSs completely exclude such an assumption.

The experimental data for BChl *c* fluorescence kinetics for all cultures investigated (*A–D*) are summarized as follows (only the fast components of BChl *c* fluorescence kinetics reflecting the rate of excitation energy transfer from BChl *c* to BChl *a* are presented):

A: $F(p = 1, 2, 3, 4) = 0.01, 0.38, 0.58, 0.03,$

$\langle p \rangle = 2.63, \tau = 40$ ps;

B: $F(p = 1, 2, 3, 4) = 0.40, 0.60, 0.00, 0.00;$

$\langle p \rangle = 1.60, \tau = 21$ ps;

C: $F(p = 1, 2, 3, 4) = 0.70, 0.30, 0.00, 0.00,$

$\langle p \rangle = 1.30, \tau = 17$ ps;

D: $F(p = 1, 2, 3, 4) = 0.90, 0.10, 0.00, 0.00,$

$\langle p \rangle = 1.10, \tau = 12$ ps.

In Fig. 11 theoretical and experimental dependences $\tau(p)$ for BChl *c* fluorescence kinetics are shown.

Theoretical dependences $\tau(p)$ (see the previous section) are presented for two different sets of parameters: $t = t^+ = 50$, $\tau_c = 650$ ps, $t^- = 0$ (curve 1) and $t = t^+ = 20$, $\tau_c = 275$ ps, $t^- = 0$ (curve 2). According to these data, the efficiency of energy transfer from the BChl *c* antenna to the baseplate (and, hence, the rate constant of fluorescence decay in this antenna) decreases with increasing chlorosome size *p*.

The $\tau(p)$ dependence is quasi-linear. This means that the $F(p)$ distribution can be characterized only by the mean value of *p*, $\langle p \rangle$ (see also the previous section). Indeed, the experimental $\tau(\langle p \rangle)$ points are very close to the calculated $\tau(p)$ curves (Fig. 11).

If we use the exact distribution $F(p)$, the time constants calculated according to Eq. 19 are $\tau = 43.7, 23.5, 17.2, 14.3$ ps (for $t = t^+ = 20$, $\tau_c = 275$ ps). They agree well with corresponding experimental values of $\tau' = 40, 21, 17, 12$ ps (see above).

For the chosen set of parameters ($t = t^+ = 20$ and $\tau_c = 275$ ps) we obtained $(K_A^A)^{-1} = 27.4$ ps, the hopping time between the antenna aggregates $(K_A^A)^{-1}/6 = 4.4$ ps (for the middle layers), $(K_A^A)^{-1}/4 = 6.6$ ps (for the upper layer), $(K_A^A)^{-1}/2 = 13.2$ ps (if there is only one layer), and time of energy transfer to the BChl790 $(qK_A^a)^{-1} = 13.7$ ps. The last-mentioned time is very close to the measured $\tau = 12$ ps value for the cell culture *D* predominantly with one layer of rods (see Fig. 8).

These hopping times correspond to the characteristic times for spectral diffusion in an inhomogeneously broadened antenna. A dynamic spectral shift with $\tau = 7$ ps was observed by Lin et al. (1991). The amplitude of this shift was 4 nm (or 80 cm^{-1}) and closely corresponded to the inhomogeneous width revealed by spectral hole-burning studies (90–100 cm^{-1}; Fetisova et al. (1994)).

Thus, the data suggest a possible mechanism of EET within the chlorosome, which implies i) the formation of a cylindrical exciton, i.e., delocalization of excitation over a tubular aggregate of six linear single or double exciton-coupled BChl *c* chains with interchain distances of ~2 nm and BChl *c* density approximating that in vivo, and ii) the Forster-type transfer of such a cylindrical exciton between the nearest tubular BChl *c* aggregate structures as well as to BChl *a* of the baseplate.

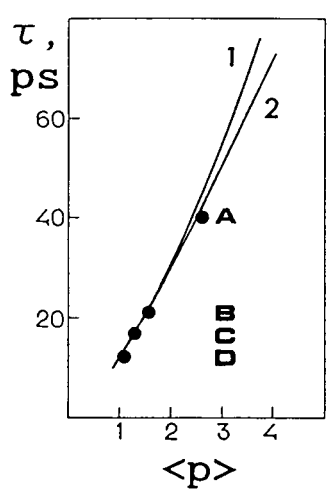

FIGURE 11 Theoretical dependences $\tau(p)$ (*solid curves 1 and 2*) and experimental points $\tau(\langle p \rangle)$ for BChl *c* fluorescence decay in living cells of each of the four *C. aurantiacus* cultures (*A–D*) shown in Figs. 7–9. Parameters for calculated dependences are listed in the text.

CONCLUSIONS

The theory of excitation energy transfer within an oligomeric-type light-harvesting antenna has been developed for the first time and, in particular, within the chlorosome of green bacteria.

A theory has been developed for a new exciton model of aggregation of chlorosomal pigments, BChl *c*, *d*, or *e*. This model of six linear exciton-coupled BChl chains with a low packing density, approximating that in vivo, and interchain distances of ~2 nm was generated to yield the key spectral features found in natural antennae, i.e., the exciton level structure, revealed by spectral hole-burning experiments, and the polarization of all the levels parallel to the long axis of the chlorosome.

None of the hitherto proposed molecular models of BChl aggregation in the chlorosome, corresponding to the two limiting cases of BChl chain packing: i) noninteracting BChl chains and ii) strongly exciton-coupled BChl chains with a high density of packing, postulating self-aggregation of pigments into a tubular macrocycle network, displays the in vivo exciton level structure of a BChl aggregate.

Using picosecond fluorescence spectroscopy, we demonstrated that the theory developed for our tubular aggregate model allows one to explain antenna-size-dependent kinetics of fluorescence decay in chlorosomal antenna, measured for intact cells of different cultures of the green bacterium *C. aurantiacus* with the different chlorosomal antenna sizes determined by electron microscopic examination of ultrathin sections of the cells.

According to our model, the energy transfer dynamics within the chlorosome implies the formation of a cylindrical exciton, delocalized over a tubular aggregate of six linear exciton-coupled BChl *c* chains, and Forster-type transfer of such a cylindrical exciton between nearest tubular BChl *c* aggregates and to BChl *a* of the baseplate.

The present research was made possible in part by grant M6R300 from the International Science Foundation, by grant 96–04-49205 from the Russian Foundation for Basic Research, and a grant from the Russian Universities Foundation. We are grateful to A. H. M. de Wit for providing us with the *C. aurantiacus* (strain Ok-70-fl).

REFERENCES

Alden, R. G., S. H. Lin, and R. E. Blankenship. 1992. Theory of spectroscopy and energy transfer of oligomeric pigments in chlorosome antennae of green photosynthetic bacteria. *J. Luminesc.* 51:51–66.

Causgrove, T. P., D. C. Brune, J. Wang, B. P. Wittmerhaus, and R. E. Blankenship. 1990. Energy transfer kinetics in whole cells and isolated chlorosomes of green photosynthetic bacteria. *Photosynth. Res.* 26: 39–48.

Chesnut, D. B., and A. Suna. 1963. Fermion behavior of one-dimensional excitons. *J. Chem. Phys.* 39:146–149.

Davydov, A. S. 1971. Theory of Molecular Excitons. Plenum Press, New York. 262 pp.

Feiler, U., D. Albouy, M. Lutz, and B. Robert. 1994. Pigment interactions in chlorosomes of various green bacteria. *Photosynth. Res.* 41:175–180.

Fetisova, Z. G. 1994. Problems of optimization of bacterial photosynthetic antenna structure. Moscow State University, Moscow. 68 pp.

Fetisova, Z. G., A. M. Freiberg, and K. E. Timpmann. 1988. Long-range molecular order as an efficient strategy for light harvesting in photosynthesis. *Nature (London).* 334:633–634.

Fetisova, Z. G., S. G. Kharchenko, and I. A. Abdourakhmanov. 1986. Strong orientational ordering of the near-infrared transition moment vectors of light-harvesting antenna bacterioviridin in chromatophores of the green photosynthetic bacterium *Chlorobium limicola. FEBS Lett.* 199:234–236.

Fetisova, Z. G., and K. Mauring. 1992. Experimental evidence of oligomeric organization of antenna bacteriochlorophyll *c* in green bacterium *Chloroflexus aurantiacus* by spectral hole burning. *FEBS Lett.* 307: 371–374.

Fetisova, Z. G., and K. Mauring. 1993. Spectral hole burning study of intact cells of green bacterium *Chlorobium limicola. FEBS Lett.* 323: 159–162.

Fetisova, Z. G., K. Mauring, and A. S. Taisova. 1994. Strongly exciton coupled BChl *e* chromophore system in chlorosomal antenna of intact cells of green bacterium *Chlorobium phaeovibrioides*: spectral hole burning study. *Photosynth. Res.* 41:205–210.

Fetisova, Z. G., K. Mauring, and A. S. Taisova. 1995. Role of delocalized exciton states of light-harvesting pigments in excitation energy transfer in natural photosynthesis. *In* Excitonic Processes in Condenced Matter. J. Singh, editor. *Proc. SPIE.* 2362:553–560.

Fetisova, Z. G., L. V. Shibaeva, and M. V. Fok. 1989. Biological expedience of oligomerization of chlorophyllous pigments in natural photosynthetic systems. *J. Theor. Biol.* 140:167–184.

Friedrich, J., and D. Haarer. 1984. Photochemical hole burning: a spectroscopic study of relaxation processes in polymers and glasses. *Angew. Chem. Int. Ed. Engl.* 23:113–140.

Forster, Th. 1965. Delocalized excitation and excitation transfer. *In* Modern Quantum Chemistry, Part III. O. Sinanoglu, editor. Academic Press, New York. 93–137.

Gillie, J. K., G. J. Small, and J. H. Golbeck. 1989. Nonphotochemical hole burning of the native antenna complex of photosystem I (PSI-200). *J. Chem. Phys.* 93:1620–1627.

Golecki, J. R., and J. Oelze. 1987. Quantitative relationship between bacteriochlorophyll content, cytoplasmic membrane structure and chlorosome size in *Chloroflexus aurantiacus. Arch. Microbiol.* 148: 236–241.

Griebenow, K., A. R. Holzwarth, F. Van Mourik, and R. Van Grondelle. 1991. Pigment organization and energy transfer in green bacteria. 2. Circular and linear dichroism spectra of protein-containing and protein-free chlorosomes isolated from *Chloroflexus aurantiacus* strain Ok-70 fl. *Biochim. Biophys. Acta.* 1058:194–202.

Holzwarth, A. R., and K. Schaffner. 1994. On the structure of bacteriochlorophyll molecular aggregates in the chlorosomes of green bacteria. A molecular modelling study. *Photosynth. Res.* 41:225–233.

Krasnovsky, A. A., and M. I. Bystrova. 1980. Self-assembly of chlorophyll aggregated structures. *BioSystems.* 12:181–194.

Lehmann, R. P., R. A. Brunisholz, and H. Zuber. 1994. Structural differences in chlorosomes from *Chloroflexus aurantiacus* grown under different conditions support the BChl *c*-binding function of the 5.7 kDa polypeptide. *FEBS Lett.* 342:319–324.

Lin, S., H. V. Van Amerongen, and W. S. Struve. 1991. Ultrafast pump-probe spectroscopy of bacteriochlorophyll *c* antennae in bacteriochlorophyll *a* containing chlorosomes from the green photosynthetic bacterium *Chloroflexus aurantiacus. Biochim. Biophys. Acta.* 1060:13–24.

Matsuura, K., M. Hirota, K. Shimada, and M. Mimuro. 1993. Spectral forms and orientation of bacteriochlorophyll *c* and *a* in chlorosomes of the green photosynthetic bacterium *Chloroflexus aurantiacus. Photochem. Photobiol.* 57:92–97.

Mimuro, M., M. Hirota, Y. Nishimura, T. Moriyama, I. Yamazaki, K. Shimada, and K. Matsuura. 1994. Molecular organization of bacteriochlorophyll in chlorosomes of the green photosynthetic bacterium *Chloroflexus aurantiacus*: studies of fluorescence depolarization accompanied by energy transfer process. *Photosynth. Res.* 41:181–191.

Mimuro, M., T. Nozawa, N. Tamai, K. Shimada, I. Yamazaki, S. Lin, R. C. Knox, B. P. Wittmershaus, D. C. Brune, and R. E. Blankenship. 1989. Excitation energy flow in chlorosome antennas of green photosynthetic bacteria. *J. Phys. Chem.* 93:7503–7509.

Nozawa, T., K. Ohtomo, M. Suzuki, H. Nakagawa, Y. Shikama, H. Konami, and Z. Wang. 1994. Structure of chlorosomes and aggregated BChl *c* in *Chlorobium tepidum* from solid state high resolution CP/MAS ^{13}C NMR. *Photosynth. Res.* 41:211–223.

Oelze, J. 1992. Light and oxygen regulation of the synthesis of bacteriochlorophylls *a* and *c* in *Chloroflexus aurantiacus. J. Bacteriol.* 174: 5021–5026.

Oelze, J., and R. C. Fuller. 1987. Growth rate and control of development of the photosynthetic apparatus in *Chloroflexus aurantiacus. Arch. Microbiol.* 148:132–136.

Olson, J. M. 1980. Chlorophyll organization in green photosynthetic bacteria. *Biochim. Biophys. Acta.* 594:33–51.

Olson, J. M., R. C. Prince, and D. C. Brune. 1977. Reaction-center complex from green bacteria. *Brookhaven Symp. Biol.* 28:238–245.

Savikhin, S., P. I. van Noort, Y. Zhu, S. Lin, R. E. Blankenship, and W. S. Struve. 1995. Ultrafast energy transfer in light-harvesting chlorosomes from the green sulfur bacterium *Chlorobium tepidum. Chem. Phys.* 194:245–258.

Savikhin, S., Y. Zhu, S. Lin, R. E. Blankenship, and W. S. Struve. 1994. Femtosecond spectroscopy of chlorosome antennas from the green photosynthetic bacterium *Chloroflexus aurantiacus. J. Phys. Chem.* 98: 10322–10334.

Smith, K. M., L. A. Kehres, and J. Fajer. 1983. Aggregation of bacteriochlorophylls *c*, *d* or *e*. Models for the antenna chlorophylls of green and brown photosynthetic bacteria. *J. Am. Chem. Soc.* 105:1387–1389.

Sprague, S. G., A. L. Staehelin, M. J. DiBartolomeis, and R. C. Fuller. 1981. Isolation and development of chlorosomes in the green bacterium *Chloroflexus aurantiacus. J. Bacteriol.* 147:1021–1031.

Staehelin, L. A., J. R. Golecki, R. C. Fuller, and G. Drews. 1978. Visualization of the supramolecular architecture of chlorosomes (*chlorobium* type vesicles) in freeze-fructured cells of *Chloroflexus aurantiacus. Arch. Microbiol.* 119:269–277.

Staehelin, L. A., J. R. Golecki, and G. Drews. 1980. Supramolecular architecture of chlorosomes (*Chlorobium* vesicles) and of their membrane attachment sites in *Chlorobium limicola. Biochim. Biophys. Acta.* 589:30–45.

Struve, W. 1995. Theory of electronic energy transfer. *In* Anoxygenic Photosynthetic Bacteria. R. E. Blankenship, M. T. Madigan, and C. E. Bauer, editors. Kluwer Academic Publishers, Dordrecht, The Netherlands. 1–17.

Van Amerongen, H., H. Vasmel, and R. Van Grondelle. 1988. Linear dichroism of chlorosomes from *Chloroflexus aurantiacus* in compressed gels and electric fields. *Biophys. J.* 54:65–76.

Van Dorssen, R. J., H. Vasmel, and J. Amesz. 1986. Pigment organization and energy transfer in the green photosynthetic bacterium *Chloroflexus aurantiacus.* II. The chlorosome. *Photosynth. Res.* 9:33–45.

Van Grondelle, R., J. P. Dekker, T. Gillbro, and V. Sundstrom. 1994. Energy transfer and trapping in photosynthesis. *Biochim. Biophys. Acta.* 1187:1–65.